Available online at www.sciencedirect.com
SCIENCE DIRECT®
Optics Communications 252 (2005) 381–396
OPTICS COMMUNICATIONS
www.elsevier.com/locate/optcom

Propagation effects in the quantum description of collective recoil lasing

R. Bonifacio [a], N. Piovella [a,*], G.R.M. Robb [b], M.M. Cola [a]

[a] *Dipartimento di Fisica, Università Degli Studi di Milano, INFM and INFN, Via Celoria 16, I-20133 Milano, Italy*
[b] *Department of Physics, University of Strathclyde, Glasgow, G4 0NG Scotland, United Kingdom*

Received 20 December 2004; received in revised form 15 April 2005; accepted 15 April 2005

Abstract

The free electron laser and collective atomic recoil laser (CARL) are examples of collective recoil lasing, where exponential amplification of a radiation field occurs simultaneously with self-bunching of an ensemble of particles (electrons in the case of the FEL and atoms in the case of the CARL). In this paper, we discuss quantum and propagation effects using a model where the particle dynamics are described quantum-mechanically in terms of a matter-wave field, which evolves self-consistently with the radiation field. The model shows that the scattered radiation evolves superradiantly both in the case where the particle ensemble is short compared to the cooperation length of the system, and where the ensemble is long compared to the cooperation length. In both short and long pulse cases there exist a classical and quantum regime of superradiant emission. For short samples in both quantum and classical regimes the superradiant pulse has a low peak intensity and is said to exhibit 'weak' superradiance. For long pulses in both quantum and classical regimes of evolution, the dynamics at the rear edge of the sample is dominated by propagation. This produces a 'strong' superradiant pulse with much higher peak intensity than that predicted by 'mean-field' or 'steady-state' models in which propagation effects are neglected.

PACS: 42.50.Fx; 41.60.Cr; 42.50.Vk

1. Introduction

The high-gain free electron laser (FEL) [1] and collective atomic recoil laser (CARL) [2–4] are at first sight very different systems, but they exhibit similar behaviors, showing self-bunching and exponential enhancement of the emitted radiation. Both systems were originally conceived in a classical framework, where the discrete nature of the recoil due to scattering of a photon by the particle was ignored, usually being masked by temperature effects in a typical experimental situation. In particular,

* Corresponding author. Tel.: +39 02 5031 7266; fax: +39 02 5031 7208.
E-mail address: nicola.piovella@mi.infn.it (N. Piovella).

0030-4018/$ - see front matter © 2005 Elsevier B.V. All rights reserved.
doi:10.1016/j.optcom.2005.04.037

CARL was originally observed in hot atomic vapors [5,6] and recently also in the presence of a friction force due to optical molasses fields [7–9]. In these experiments, the particle motion can be described classically. However, new experiments using Bose–Einstein condensates (BEC) [10–13] have made it necessary to describe the center-of mass motion of the atoms in CARL quantum mechanically [14–20]. The model has shown the existence of new quantum dynamical regimes of CARL [17], in which the momentum changes by discrete units of the photon recoil momentum $2\hbar k$, where k is the wave number of the photon. The CARL experiments with BECs have been performed in the superradiant regime to date [10–13], where, in the absence of an optical cavity, the radiation escapes rapidly from the atomic sample. This regime has been described using a 'mean field' model, in which a phenomenological damping term inversely proportional to the length of the atomic sample is added to the field equation. However, a rigorous description of the superradiant regime requires the solution of the exact propagation equation of the radiation field. Propagation effects may also be important for CARL when the radiation is stored in an optical ring cavity [21].

Propagation effects are known to be of great importance in single-pass high-gain FELs [22,23]. In fact, different superradiant regimes have been predicted, with peak intensity proportional to N^2 (where N is the number of particles) both for electron bunches shorter ('weak superradiance') or longer ('strong superradiance') than the cooperation length L_c of the system. Moreover, propagation effects are fundamental in the self-amplified spontaneous emission (SASE) regime, where the initial incoherent shot-noise in the electron bunch is amplified to generate a random superposition of high-intensity superradiant spikes [24]. Hence, a quantum description of the superradiant and SASE regimes is timely and of great interest for the current experimental realization of a future X-ray coherent source [25,26].

In this work we give a quantum description of the propagation effects both for FELs and CARLs, described by the same system of partial differential equations for dimensionless variables [27]. The particle dynamics are described quantum-mechanically in terms of a matter-wave field obeying a Schrödinger equation coupled self-consistently with the Maxwell equation for the radiation field amplitude [28]. The model is based on multiple-scaling perturbation theory, in which the particle distribution evolves on the scale of the radiation wavelength, whereas the radiation amplitude evolves on a spatial scale much slower than the radiation wavelength [29]. The model depends on a single collective parameter $\bar{\rho}$ which rules the transition between the quantum and classical regimes, and which represents the amount of recoil momentum transferred to the particle sample. The classical regime is recovered for large values of $\bar{\rho}$ when the change of particle momentum is much larger than the single-photon recoil $\hbar k$. We demonstrate that in this limit the quantum model reduces to the classical model, in which the equation for the Wigner function of the particle sample reduces to the Vlasov equation for the classical phase-space distribution. Conversely, in the quantum regime (small value of $\bar{\rho}$), the model reduces to the well-known Maxwell–Bloch equations [32] for a two-state system, where the two states are the initial momentum state and the state with momentum displaced by the photon recoil momentum.

The model predicts that, both in the case where the particle sample is short or long compared to the cooperation length of the system, there exists a classical and a quantum regime of superradiance, with peak intensity proportional to N^2, where N is the number of particles. In the case of classical superradiance, many momentum states participate in the emission and the particle momentum changes by an amount much larger than $\hbar k$. Conversely, in the case of quantum superradiance, only two momentum states participate in the interaction and each particle may scatters only a single photon. For short samples in both the quantum and classical regimes, the particle emits a 'weak' superradiant pulse with a main peak followed by several peaks of smaller intensity (ringing). For long samples, an initially 'weak' superradiant pulse develops near the rear edge of the sample and is amplified when it propagates toward the front edge of the sample ('strong superradiance'). We show that our model admits two different

self-similar solutions both for the classical and quantum superradiant regimes, in which the peak of the radiation intensity is proportional to N^2 in both the classical and quantum regimes, and the scattered pulse width is inversely proportional to $\sqrt{N}$ in the classical regime and to N in the quantum regime.

The paper is organized as follows. In Section 2, we introduce the quantum model for collective recoil lasing with equations written in a universal form appropriate to describe both FEL and CARL systems. In Section 3, we present the quantum propagation model introducing two different spatial scales and we discuss the classical and quantum limits of this model. In Section 4, we show the existence of soliton-like solutions of the propagation equations, describing the classical and quantum superradiant regimes. In Section 5, we present numerical results obtained by integrating the propagation equations and we discuss the quantum and classical regimes of superradiance in the short and long sample cases. Conclusions are summarized in Section 6.

2. A unified model for CARL and FEL

The physics of FEL and CARL appear at first to be quite different. The first describes a relativistic high current electron beam with energy $mc^2\gamma_0$, injected in a magnet ('wiggler') with a transverse, static magnetic field B_w and periodicity λ_w, which radiates in the forward direction at the wavelength $\lambda \sim \lambda_w(1 + a_w^2)/2\gamma_0^2$, where $a_w = eB_w/mc^2k_w$ is the wiggler parameter and $k_w = 2\pi/\lambda_w$ [23]. Instead, CARL consists of a collection of two-level atoms, driven by a far-detuned pump laser of frequency ω_p, which radiates at the frequency $\omega \sim \omega_p$ in the direction opposite to the pump [2]. In both cases the radiation process arises from a collective instability which originates a symmetry breaking in the spatial distribution of the particles, i.e. a self-bunching of particles which group in regions smaller than the wavelength.

The quantum-mechanical dynamics of both FELs and CARLs can be described by a Schrödinger equation for the 'matter-wave' field Ψ [28], coupled self-consistently with the equation for the radiation field amplitude A:

$$i\frac{\partial\Psi(\theta,\bar{t})}{\partial\bar{t}} = -\frac{1}{\bar{\rho}}\frac{\partial^2\Psi(\theta,\bar{t})}{\partial\theta^2} - \frac{i\bar{\rho}}{2}\left[A(\theta,\bar{t})e^{i\theta} - \text{c.c.}\right]\Psi(\theta,\bar{t}), \tag{1}$$

$$\left(\frac{\partial}{\partial\bar{t}} + \frac{1}{\epsilon}\frac{\partial}{\partial\theta}\right)A(\theta,\bar{t}) = |\Psi(\theta,\bar{t})|^2e^{-i\theta} + i\frac{\delta}{\bar{\rho}}A(\theta,\bar{t}), \tag{2}$$

where θ is the phase of the particle, $\bar{t}$ is the dimensionless time, $|A|^2 = (2/N\bar{\rho})|a|^2$, where $|a|^2$ is the average number of photons in the volume V, and $|\Psi(\theta,\bar{t})|^2$ is the space-time dependent particle density, normalized to unity. Notice that the dynamics described by Eqs. (1) and (2) depend only on the parameter $\bar{\rho}$ and on the detuning δ. The meaning of the variables in Eqs. (1) and (2) is described separately for FELs and CARLs as follows.

2.0.1. FEL variables

For FELs $\bar{\rho} = 2\bar{\rho}_F$, where

$$\bar{\rho}_F = \left(\frac{mc\gamma_r}{\hbar k}\right)\rho_F \tag{3}$$

is the quantum FEL parameter,

$$\rho_F = \frac{1}{\gamma_r}\left(\frac{a_w}{4ck_w}\right)^{2/3}\left(\frac{e^2n}{m\epsilon_0}\right)^{1/3} \tag{4}$$

is the BPN parameter [1] and $n = N/V$ is the average electron density. Typical values of ρ_F are 10^{-2}–10^{-3} in the high-gain regime, whereas usually $\bar{\rho} \gg 1$ due to the large value of the quantum parameter $mc\gamma_r/\hbar k$. The other parameters are

$$\delta = \frac{2mc(\gamma_0 - \gamma_r)}{\hbar k}, \tag{5}$$

$$\theta = (k + k_w)z - ckt = (k + k_w)(z - v_rt), \tag{6}$$

$$\bar{t} = \frac{z}{L_g}, \quad z_1 = \epsilon\theta = \frac{z - v_rt}{\beta_rL_c}, \tag{7}$$

$$\epsilon = 2\rho_F = \frac{\lambda}{2\pi L_c}, \tag{8}$$

where $v_r = c\beta_r = ck/(k + k_w)$ is the electron resonant velocity and $\gamma_r = (1 - \beta_r^2)^{-1/2}$ is the resonant energy in mc^2 units. The wiggler length z is expressed in units of the gain length $L_g = (2k_w\rho_F)^{-1} = \lambda_w/4\pi\rho_F$, whereas the coordinate along the electron bunch $z - v_r t$ is expressed in units of the cooperation length $L_c = (2k\rho_F)^{-1} = \lambda/4\pi\rho_F$.

2.0.2. CARL variables

For CARLs $\bar{\rho} = \bar{\rho}_C$, where

$$\bar{\rho}_C = \left(\frac{S_0 g\sqrt{n}}{\omega_R}\right)^{2/3} \tag{9}$$

is the CARL parameter [2–4]. The other parameters are

$$\delta = \frac{\omega_p - \omega}{\omega_R}, \tag{10}$$

$$\theta = 2kz, \tag{11}$$

$$\bar{t} = \frac{ct}{L_c}, \quad z_1 = \epsilon\theta = \frac{z}{L_c}, \tag{12}$$

$$\epsilon = \left(\frac{\omega_R}{2\omega}\right)\bar{\rho}_C = \frac{\lambda}{4\pi L_c}, \tag{13}$$

where n is the average atomic density, $\omega_R = 2\hbar k^2/m$ is the recoil frequency, $L_c = c/\omega_R\bar{\rho}_C$ is the cooperation length,

$$g = \sqrt{\frac{\omega d^2}{2\hbar\epsilon_0}}, \tag{14}$$

is the coupling constant, d is the dipole matrix element, $S_0 = \Delta\Omega/[2(\Gamma^2 + \Delta^2 + \Omega^2)]$, Ω is the pump Rabi frequency, Δ is the pump-atom detuning and Γ is the natural decay constant of the atomic transition [4]. In CARL experiments, usually $\Delta \gg \Gamma, \Omega$, so that $S_0 \approx \Omega/2\Delta \ll 1$. However, assuming $\Delta \gg \Gamma$, S_0 may be maximized to 1/4 for $\Delta \sim \Omega$. In the CARL experiments, atoms have a zero average velocity, so there is not a distinction between the gain and cooperation lengths as occurs in the FEL and typically, $\bar{\rho}_C \gg 1$ [10–12].

Notice that both in FELs and CARLs, $\bar{\rho}$ scales as $n^{1/3}$, i.e. as the reciprocal of the inter-particle distance.

3. Propagation model for quantum collective recoil lasing

3.1. Basic equations

For typical values of the parameters, for CARLs $\epsilon \sim 10^{-8}$, whereas for FELs $\epsilon \sim 10^{-3}$. Furthermore, because of the rapidly oscillating factor $e^{i\theta}$ in Eqs. (1) and (2) it is not convenient to solve these equations as they stand. Instead, we use a multi-scaling approach [33] developing a perturbation expansion of Eqs. (1) and (2) in the limit of small ϵ. This technique allows us to separate the short spatial evolution of the system on the scale of the optical wavelength as described by θ, from the much longer evolution of the system on the scale of the cooperation length as described by $z_1 = \epsilon\theta$, treating θ and z_1 as independent variables. A similar treatment has been applied to describe light propagation in the classical FEL model [29].

Applying the multiple scaling argument to Eqs. (1) and (2) (see Appendix A for details) one obtains the following propagation equations:

$$i\frac{\partial\Psi(\theta, z_1, \bar{t})}{\partial\bar{t}} = -\frac{1}{\bar{\rho}}\frac{\partial^2}{\partial\theta^2}\Psi(\theta, z_1, \bar{t}) - \frac{i\bar{\rho}}{2}\left[A(z_1, \bar{t})e^{i\theta} - \text{c.c.}\right]\Psi(\theta, z_1, \bar{t}), \tag{15}$$

$$\frac{\partial A(z_1, \bar{t})}{\partial\bar{t}} + \frac{\partial A(z_1, \bar{t})}{\partial z_1} = \frac{1}{2\pi}\int_0^{2\pi} d\theta\,|\Psi(\theta, z_1, \bar{t})|^2 e^{-i\theta} + i\frac{\delta}{\bar{\rho}}A(z_1, \bar{t}), \tag{16}$$

Eqs. (15) and (16) form the desired set of equations describing light propagation in the quantum collective recoil lasing model, i.e. yield the spatio-temporal evolution of the radiation field amplitude $A(z_1, \bar{t})$ and the matter wave field $\Psi(\theta, z_1, \bar{t})$. Notice that the wavefunction Ψ depends only parametrically on z_1 as a consequence of the spatial dependence of the field amplitude $A(z_1, \bar{t})$. The model previously used to describe the quantum regime of the FEL and

CARL [15,17,27] is recovered from Eqs. (15) and (16) neglecting the derivative with respect to z_1 and the dependence on z_1 in the field amplitude, i.e. the variation of the field amplitude on the sample of particles. This is appropriate for FELs when the slippage (due to the difference between the light and electron velocities) is negligible, and for CARLs when the atoms are enclosed in a high-finesse ring cavity, as in the experiments of [5–7].

The recent experiments on superradiant Rayleigh scattering from a BEC [10,12] have been previously described using the 'mean-field model', in which the partial derivative $\partial A(z_1,\bar{t})/\partial z_1$ in Eq. (16) is approximated by a damping term $-\kappa A(\bar{t})$, where $A(\bar{t})$ is the spatially averaged field and κ is the radiation loss, inversely proportional to the photon escape time from the atomic sample. The 'mean field' model correctly describes the field evolution in a high-finesse ring cavity, where $\kappa \propto cT/L_{\rm cav}$, T is the mirror transmission coefficient and $L_{\rm cav}$ is the cavity length. In free space, the 'mean field' model provides only an approximate description of the field evolution. In particular, it does not describe the ringing oscillation of the scattered field intensity after the first peak. Instead, this feature is described by the exact propagation model of Eqs. (15) and (16) as will be discussed in the following sections. On the other hand, Eqs. (15) and (16) provide a quantum extension of the classical model with propagation for FELs [29,22,23], used to describe superradiant and SASE regimes. The solution of Eqs. (15) and (16) depends on the dimensionless length $\overline{L} = L/L_{\rm c}$, where L is the length of the particle sample.

Eqs. (15) and (16) describe the pulsed regime of CARLs and FELs for a particle sample that initially is unbunched on the scale of the radiation wavelength, i.e. such that $\Psi(\theta,z_1,\bar{t}=0)$ is independent of θ. Since θ enters Eq. (15) only through the periodic function $e^{i\theta}$, $\Psi(\theta,z_1,\bar{t})$ is a periodic function of θ. It can be shown that Eq. (15) implies:

$$\frac{\partial}{\partial \bar{t}}\int_0^{2\pi} d\theta\,|\Psi(\theta,z_1,\bar{t})|^2 = 0. \tag{17}$$

Hence, the dimensionless density profile $I_0(z_1) = \int_0^{2\pi} d\theta\,|\Psi|^2$ is independent on $\bar{t}$. This means that the spatial distribution of the particles does not change appreciably on the slow scale z_1 during the interaction with the radiation.

3.2. Wigner description and classical limit

In general, the classical limit for CARLs and FELs is obtained when the change of momentum of the particles is much larger than the quantum photon recoil $\hbar k$. This can be seen more easily introducing the Wigner function of the particle distribution.

Let us consider the standard definition of the Wigner function associated with the wave function $\Psi(\theta,z_1,\bar{t})$:

$$W(\theta,p,z_1,\bar{t}) = \frac{1}{2\pi}\int_{-\infty}^{+\infty} d\xi e^{-i\xi p}\Psi^* \times\left(\theta-\frac{\xi}{2},z_1,\bar{t}\right)\Psi\left(\theta+\frac{\xi}{2},z_1,\bar{t}\right), \tag{18}$$

where p is the canonical momentum conjugate to θ (i.e. $p = mc(\gamma-\gamma_0)/\hbar k$ for FEL and $p = p_z/(2\hbar k)$ for CARL, where p_z is the linear momentum along the z-axis). Note that

$$\int_{-\infty}^{+\infty} dp\,W(\theta,p,z_1,\bar{t}) = |\Psi(\theta,z_1,\bar{t})|^2. \tag{19}$$

It has been shown [27] that Eqs. (15) and (16) are equivalent to the following equations for the quasi-probability distribution $W(\theta,\bar{p},z_1,\bar{t})$ and the field A:

$$\frac{\partial W(\theta,\bar{p},z_1,\bar{t})}{\partial \bar{t}} + \bar{p}\frac{\partial W(\theta,\bar{p},z_1,\bar{t})}{\partial\theta} - \frac{\bar{\rho}}{2}\left(Ae^{i\theta}+A^*e^{-i\theta}\right) \times\left[W\left(\theta,\bar{p}+\frac{1}{\bar{\rho}},z_1,\bar{t}\right) - W\left(\theta,\bar{p}-\frac{1}{\bar{\rho}},z_1,\bar{t}\right)\right] = 0, \tag{20}$$

$$\frac{\partial A}{\partial \bar{t}} + \frac{\partial A}{\partial z_1} = \frac{1}{2\pi}\int_{-\infty}^{+\infty} d\bar{p}\int_{-\infty}^{+\infty} d\theta\,W(\theta,\bar{p},z_1,\bar{t})e^{-i\theta} + i\frac{\delta}{\bar{\rho}}A, \tag{21}$$

where $\bar{p} = (2/\bar{\rho})p$. On the right hand side of Eq. (20), the incremental ratio

$$[W(\theta,\bar{p}+1/\bar{\rho},z_1,\bar{t}) - W(\theta,\bar{p}-1/\bar{\rho},z_1,\bar{t})]/(2/\bar{\rho}) \to \partial W(\theta,\bar{p},z_1,\bar{t})/\partial\bar{p}$$

when $\bar{\rho}\to\infty$. Hence, for large values of $\bar{\rho}$, Eq. (20) becomes the Vlasov equation:

$$\frac{\partial W(\theta,\bar{p},z_1,\bar{t})}{\partial \bar{t}}+\bar{p}\frac{\partial W(\theta,\bar{p},z_1,\bar{t})}{\partial \theta}-\left(A\mathrm{e}^{\mathrm{i}\theta}+A^{*}\mathrm{e}^{-\mathrm{i}\theta}\right)\times\frac{\partial W(\theta,\bar{p},z_1,\bar{t})}{\partial \bar{p}}=0. \tag{22}$$

Eqs. (21) and (22) form the classical CARL-FEL model extended to include propagation [29]. More precisely, Eq. (22) holds for $\bar{p}\gg 1/\bar{\rho}$. Since the momentum in units of the photon recoil momentum is $p=(\bar{\rho}/2)\bar{p}$, the condition $\bar{p}\gg 1/\bar{\rho}$ implies that in the classical limit the momentum transferred to the particles is much larger than the photon recoil momentum. For CARL, it means $p_z\gg 2\hbar k$, for FEL, $mc(\gamma-\gamma_0)\gg\hbar k$. In this limit, the quantum recoil effect due to the single photon scattering process is negligible.

3.3. Momentum expansion and collective recoil instability

Assuming that $\Psi(\theta,z_1,\bar{t})$ is a periodic function of θ, it can be expanded in a Fourier series:

$$\Psi(\theta,z_1,\bar{t})=\sum_{n=-\infty}^{\infty}c_n(z_1,\bar{t})\mathrm{e}^{\mathrm{i}n\theta}. \tag{23}$$

By inserting Eq. (23) into Eqs. (15) and (16), we obtain

$$\frac{\partial c_n}{\partial \bar{t}}=-\frac{\mathrm{i}n^2}{\bar{\rho}}c_n-\frac{\bar{\rho}}{2}\left(Ac_{n-1}-A^{*}c_{n+1}\right), \tag{24}$$

$$\frac{\partial A}{\partial \bar{t}}+\frac{\partial A}{\partial z_1}=\sum_{n=-\infty}^{\infty}c_nc_{n-1}^{*}+\mathrm{i}\frac{\delta}{\bar{\rho}}A, \tag{25}$$

Eqs. (24) and (25) are our working equations and their numerical analysis will be discussed in the next section. Note that from Eq. (23) it follows that $|c_n|^2$ is the probability that a particle has a momentum $p=n$ in units of the photon recoil momentum,

$$b=\sum_{n=-\infty}^{\infty}c_nc_{n-1}^{*} \tag{26}$$

is the bunching parameter and

$$\langle p\rangle=\sum_{n=-\infty}^{\infty}n|c_n|^2 \tag{27}$$

is the average momentum. The stability analysis of Eqs. (24) and (25) has been carried out in [15,17,20] for the case with no propagation. We assume the equilibrium state with no field, $A=0$, and all the particles in the state $n=0$, with $|c_0|^2=1$ and $|c_m|^2=0$ for all $m\neq 0$. This is equivalent to assuming that the temperature of the system is zero and there is no momentum spread. This equilibrium state can be unstable when the dispersion relation

$$\left(\lambda-\frac{\delta}{\bar{\rho}}\right)\left(\lambda^2-\frac{1}{\bar{\rho}^2}\right)+1=0, \tag{28}$$

has complex roots. In Fig. 1 we plot the imaginary part of λ as a function of $\delta/\bar{\rho}$ for different values of $\bar{\rho}$. The classical limit is obtained for $\bar{\rho}\gg 1$ (see Fig. 1(a)). In this case, the system is unstable for $\delta\lesssim 2\bar{\rho}$, with maximum instability rate $\mathrm{Im}\,\lambda=\sqrt{3}/2$ at $\delta=0$. When $\bar{\rho}$ is smaller than unity (Fig. 1(c)–(f)), the instability rate decreases and the peak of $\mathrm{Im}(\lambda)$ moves around $\delta=1$, with peak value $\mathrm{Im}\,\lambda=\sqrt{\bar{\rho}/2}$ and full width on δ equal to $(2\bar{\rho})^{3/2}$. As discussed in [17,20], for $\bar{\rho}\gg 1$ the particles have almost the same probability of transition from the momentum state $n=0$ to $n=1$ or $n=-1$ (i.e. $|c_1|^2\sim|c_{-1}|^2$), absorbing or emitting a photon. On the contrary, in the case $\bar{\rho}\leqslant 1$, $|c_1|^2\ll|c_{-1}|^2$, i.e. the particles can only emit a photon without absorption.

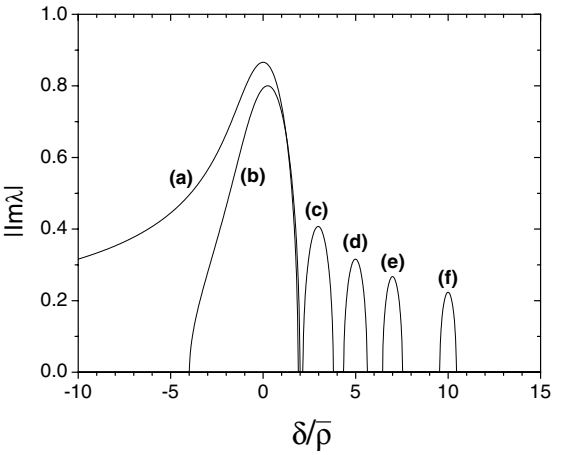

Fig. 1. Imaginary part of the unstable root of the cubic equation (28) vs. $\delta/\bar{\rho}$, for $1/\bar{\rho}=0$ (a), 0.5 (b), 3 (c), 5 (d), 7 (e) and 10 (f).

We now briefly discuss the meaning of the resonance $\delta = 1$. For CARLs, from the definition (10), it means $\omega = \omega_p - \omega_R$, i.e. the frequency of the emitted photon is red-shifted by the recoil frequency ω_R. For FELs, the resonance condition $\delta = 1$ means, from the definition (5), $mc^2(\gamma_0 - \gamma_r) = \hbar\omega/2$, which corresponds to the center of the emission line in the FEL [30,31].

3.4. Quantum limit and two-state approximation

As shown by the linear stability analysis discussed above, the quantum regime of the CARL-FEL system occurs for small value of $\bar{\rho}$, when a particle scatters only a single photon. In this limit, the dynamics is that of a system with only two momentum states, i.e. the initially occupied state with $n = 0$ and the recoiling state with $n = -1$. In this limit, Eqs. (24) and (25), after defining the 'polarization' $S = c_0 c_{-1}^* \exp[i(\delta/\bar{\rho})\bar{t}]$ and the 'population difference' $D = |c_0|^2 - |c_{-1}|^2$, reduce to the Maxwell–Bloch equations for a two-state system [32]:

$$\frac{\partial}{\partial \bar{t}} S(z_1, \bar{t}) = -i\Delta S(z_1, \bar{t}) + \frac{\bar{\rho}}{2} \overline{A}(z_1, \bar{t}) D(z_1, \bar{t}), \tag{29}$$

$$\frac{\partial}{\partial \bar{t}} D(z_1, \bar{t}) = -\bar{\rho}\left[\overline{A}(z_1, \bar{t})^* S(z_1, \bar{t}) + \text{c.c.}\right], \tag{30}$$

$$\frac{\partial \overline{A}}{\partial \bar{t}} + \frac{\partial \overline{A}}{\partial z_1} = S(z_1, \bar{t}), \tag{31}$$

where $\Delta = (\delta - 1)/\bar{\rho}$ and $\overline{A} = A \exp[-i(\delta/\bar{\rho})\bar{t}]$. Notice that in the quantum limit the average momentum is $\langle p \rangle = -|c_{-1}|^2 = (D - 1)/2$. Changing our time variable to $z_2 = \bar{t} - z_1 = (ct - z)/L_c$, the spatial and temporal derivatives become:

$$\frac{\partial}{\partial \bar{t}} \to \frac{\partial}{\partial z_2}, \quad \frac{\partial}{\partial \bar{t}} + \frac{\partial}{\partial z_1} \to \frac{\partial}{\partial z_1}. \tag{32}$$

Assuming resonance in Eqs. (29)–(31) (i.e. $\Delta = 0$), $\overline{A}$ and S can be assumed to be real. Then, introducing the Bloch angle $\phi(z_1, z_2)$ such that $S(z_1, z_2) = (1/2)\sin\phi(z_1, z_2)$ and $D(z_1, z_2) = \cos\phi(z_1, z_2)$, Eqs. (29)–(31) can be combined to give the so-called sine-Gordon equation [34],

$$\frac{\partial^2 \phi(z_1, z_2)}{\partial z_1 \partial z_2} = \frac{\bar{\rho}}{2} \sin\phi(z_1, z_2), \tag{33}$$

and

$$\frac{\partial \phi}{\partial z_2} = \bar{\rho}\overline{A}. \tag{34}$$

Notice that the parameter $\bar{\rho}$ in Eqs. (29)–(31) may be eliminated redefining the variables as $A' = \sqrt{\bar{\rho}}\bar{A}$, $t' = \sqrt{\bar{\rho}}\bar{t}$, $z_1' = \sqrt{\bar{\rho}} z_1$ and $\Delta' = \Delta/\sqrt{\bar{\rho}}$. With this quantum universal scaling the cooperation length becomes $L_c' = L_c/\sqrt{\bar{\rho}} \propto 1/\sqrt{N}$. Furthermore, with this new scaling, Eq. (1) (or equivalently Eq. (15)) can be interpreted as a Schrödinger equation for a single particle with a 'mass' $\bar{\rho}^{3/2}$ in a self-consistent pendulum potential. This provides an intuitive interpretation of the classical limit, that holds when the particle's 'mass' is large.

4. Soliton-like solutions for the classical and quantum regimes

We now demonstrate that both the classical equations (21) and (22) and the quantum equations (33) and (34) admit a self-similar solution in which the field amplitude $A(z_1, \bar{t})$ is proportional to the spatial coordinate z_1.

Assuming that the medium extends from $z_1 = 0$ to $z_1 = \overline{L}$, the appropriate boundary condition for the field equation (21) is $A(z_1 = 0, z_2 > 0) = 0$. In fact, the pulse propagates only forward, so it is zero at the trailing-edge $z_1 = 0$. The boundary condition for the particle equation (22) is $W(\theta, \bar{p}, z_1, z_2 = 0) = W_0(\theta, \bar{p})$, since the particle does not radiate before the arrive of the pulse. It is already known for FELs that Eqs. (21) and (22) admit a solution of the form

$$A(z_1, z_2) = z_1 A_1(y), \tag{35}$$

$$W(\theta, \bar{p}, z_1, z_2) = \sqrt{z_1} W_1(\theta, p_1, y), \tag{36}$$

where

$$y = \sqrt{z_1} z_2, \quad p_1 = \frac{\bar{p}}{\sqrt{z_1}}, \tag{37}$$

and $A_1(y)$ and $W_1(\theta, p_1, y)$ are solutions of the following equations:

$$\frac{\partial W_1}{\partial y} + p_1 \frac{\partial W_1}{\partial \theta} - \left(A_1 e^{i\theta} + A_1^* e^{-i\theta}\right) \frac{\partial W_1}{\partial p_1} = 0, \tag{38}$$

$$\frac{y}{2}\frac{\mathrm{d}A_1}{\mathrm{d}y}+A_1=\frac{1}{2\pi}\int_{-\infty}^{+\infty}\mathrm{d}p_1\int_{-\infty}^{+\infty}\mathrm{d}\theta\, W_1\mathrm{e}^{-\mathrm{i}\theta}, \tag{39}$$

which can also be expressed as particle equations [35,23]:

$$\frac{\mathrm{d}\theta}{\mathrm{d}y}=p_1, \tag{40}$$

$$\frac{\mathrm{d}p_1}{\mathrm{d}y}=-\left(A_1\mathrm{e}^{\mathrm{i}\theta}+A_1^*\mathrm{e}^{-\mathrm{i}\theta}\right), \tag{41}$$

$$\frac{y}{2}\frac{\mathrm{d}A_1}{\mathrm{d}y}+A_1=\langle\mathrm{e}^{-\mathrm{i}\theta}\rangle. \tag{42}$$

In Fig. 2(a) and (c) we plot the intensity $|A_1|^2$ and the average momentum $\langle p_1\rangle$, as defined in Eqs. (35) and (37), as a function of the self-similar coordinate $y=\sqrt{z_1}z_2$, as obtained from the numerical solution of Eqs. (40)–(42).

On the other hand, self-similarity has been demonstrated also for the sine-Gordon equation (33) [34]. We assume a small initial tipping angle, i.e. $\phi(z_1, z_2=0)=\phi_0$, as a boundary condition for Eq. (33). Furthermore, by integrating Eq. (34) on z_2 with $\overline{A}(z_1=0,z_2)=0$, one obtains also $\phi(0,z_2)=\phi(z_1,0)=\phi_0$. These boundary conditions are consistent with a solution of the form $\phi(z_1, z_2)=\Phi(x)$, where

$$x=(\bar{\rho}/2)z_1z_2. \tag{43}$$

With the change of variable (43), the partial differential equation (33) is reduced to the ordinary differential equation

$$x\Phi''+\Phi'-\sin\Phi=0, \tag{44}$$

with boundary conditions $\Phi(0)=\phi_0$ and $\Phi'(0)=0$, whereas the field amplitude is

$$A(z_1,z_2)=z_1A_2(x)=\frac{z_1}{2}\Phi'(x). \tag{45}$$

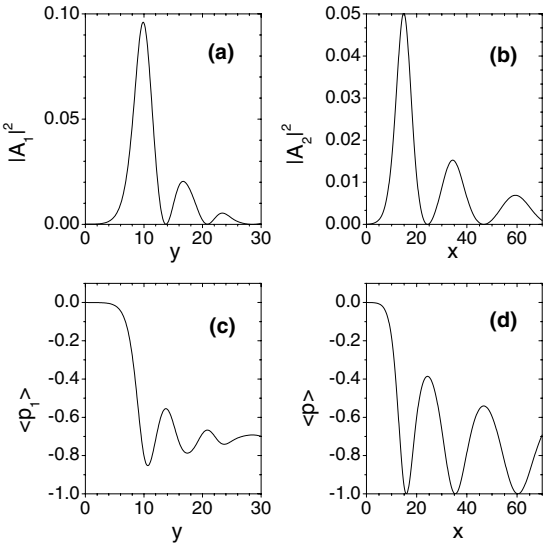

Fig. 2. Classical and quantum self-similar solutions. Classical regime: $|A_1|^2$ (a), and $\langle p_1\rangle=\langle\bar{p}\rangle/\sqrt{z_1}$ (c), as a function of $y=\sqrt{z_1}z_2$, calculated from the numerical solution of Eqs. (40)–(42). Quantum regime: $|A_2|^2$ (b), and $\langle p\rangle$ (d), as a function of $x=(\bar{\rho}/2)z_1z_2$, calculated from the numerical solution of Eq. (44).

Fig. 2(b) and (d) plot the quantum self-similar solution $|A_2|^2$ (as defined in Eq. (45)) and $\langle p\rangle=(D-1)/2=-\sin^2(\Phi/2)$ as a function of the self-similar coordinate $x=(\bar{\rho}/2)z_1z_2$, as obtained from the numerical solution of Eq. (44).

It is remarkable to note that in both the classical and quantum regimes the dimensionless amplitude A of the field at the front edge of the particle beam ($z_1=\overline{L}$) is proportional to $\overline{L}\propto N^{1/3}$, so that the number of emitted photons $|a|^2=(N\bar{\rho}/2)|A|^2\propto N^2$, i.e. is superradiant. From the definition of the self-similar variables x and y given by Eqs. (43) and (37), one can see that for $z_1=\overline{L}$ the width of the radiation pulse scales as $\overline{L}^{-1/2}$ in the classical regime and as $2/\bar{\rho}\overline{L}$ in the quantum regime. These results apply to the recent experiments on the superradiant regime of CARL with a BEC, where $\overline{L}\ll 1$ [10,12]. Since in the classical regime the minimum of $\langle\bar{p}\rangle$ is approximately $-\overline{L}^{1/2}$ at the front edge of the sample $z_1=\overline{L}$ (as can be obtained from Eq. (37) and from Fig. 2(c)), then the minimum momentum in units of the photon recoil momentum is $\langle p\rangle\approx-(\bar{\rho}/2)\overline{L}^{1/2}$. Hence, the classical regime in CARL superradiance occurs for $\bar{\rho}\overline{L}^{1/2}\gg 1$, i.e., using the definition (9), for $G_{\mathrm{SR}}\gg\omega_{\mathrm{R}}$, where $G_{\mathrm{SR}}=S_0^2g^2n(L/c)$ is the superradiant gain [17].

The classical self-similar solution (35) has already been predicted for single-pass high-gain FELs in the long-pulse limit ($L\gg L_{\mathrm{c}}$), yielding the 'strong superradiant' regime [22,23] and the 'self amplified

spontaneous emission' (SASE) regime [24] when the emission starts from shot noise. In the following, we will show numerically the existence of a quantum limit of the strong superradiant regime, provided that the initial energy spread is below the photon recoil limit, i.e. $mc(\delta\gamma)_0 < \hbar k$.

5. Numerical analysis

5.1. Short samples – weak superradiance

We now investigate the collective recoil instability in short samples, where by 'short' we mean that the particle sample length, L, is much shorter than the cooperation length of the system, L_c, so that $\overline{L} \ll 1$. Mean field models have previously been used [4,17,37] to describe the collective recoil instability in such short samples phenomenologically. These models demonstrate that the collective recoil instability results in the generation of a superradiant pulse, with peak intensity $\propto N^2$. Recent experiments involving Superradiant Rayleigh scattering from a BEC [10–12] are examples of this short sample regime, as they can be described in term of a CARL instability [19,36] in a short atomic sample where $\overline{L} \ll 1$.

We now investigate the evolution of the collective recoil instability in a short sample $\overline{L} \ll 1$ including the full spatio-temporal evolution of the particle and optical fields using the momentum eigenstate amplitude equations (24) and (25) both in the classical and quantum regimes. In the simulations which follow, the interaction is initiated by a small initial bunching in the sample. The initial conditions for all the simulations are $A(z_1, \bar{t} = 0) = 0$, $c_{-1}(z_1, \bar{t} = 0) = b_0$ and $c_0(z_1, \bar{t} = 0) = \sqrt{1 - b_0^2}$, where $b_0 = 0.01$ so that from Eq. (26) $b(z_1, \bar{t} = 0) \approx b_0$.

5.1.1. Classical limit

Fig. 3 shows the evolution of the scattered field intensity $|A|^2$, the bunching parameter b (26) and the average momentum $\langle p \rangle$ (27) as a function of $\bar{t}$ at the front edge of the particle sample ($z_1 = \overline{L}$) for the case where $\overline{L} = 0.1$, $\bar{\rho} = 10$ and $\delta = 0$. It can be seen that the scattered field is emitted as a large pulse followed by smaller pulses and that there is a strong density modulation or bunching at the front of the sample. Although mean field models also predict the appearance of the first pulse, the additional pulses, or 'ringing', appear only when the effects of propagation are fully described. The behavior of the field intensity $|A|^2$ and the mean momentum $\langle p \rangle$ in Fig. 3 is in agreement with that predicted by the self-similar solution (35) shown in Fig. 2(a) and (c).

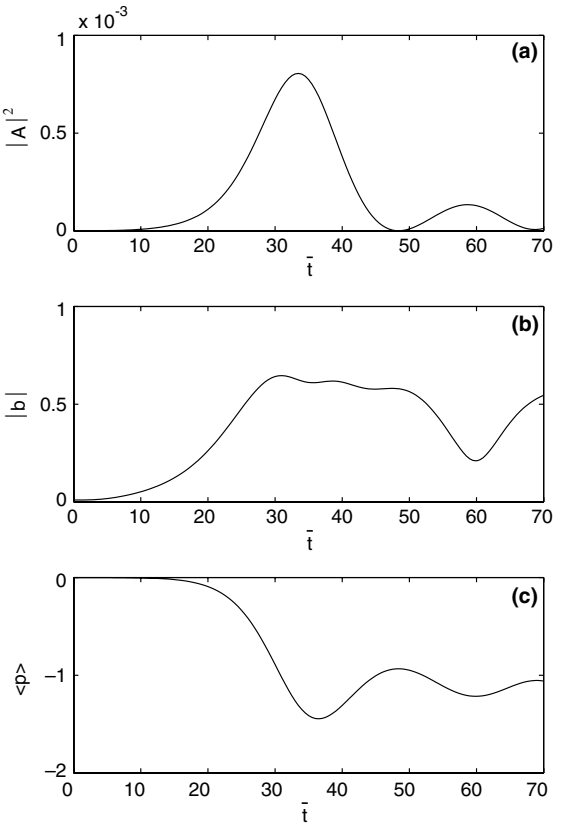

Fig. 3. (a) $|A|^2$, (b) $|b|$ and (c) $\langle p \rangle$ as a function of $\bar{t}$ at $z_1 = \overline{L}$ when $\overline{L} = 0.1$, $\bar{\rho} = 10$ and $\delta = 0$.

Fig. 4 shows the momentum distribution at the front edge of the particle sample ($z_1 = \overline{L}$) at times well before the first maximum of the scattered field intensity (Fig. 4(a)), close to the intensity maximum (Fig. 4(b)) and well after the first maximum of the scattered intensity (Fig. 4(c)) for the same

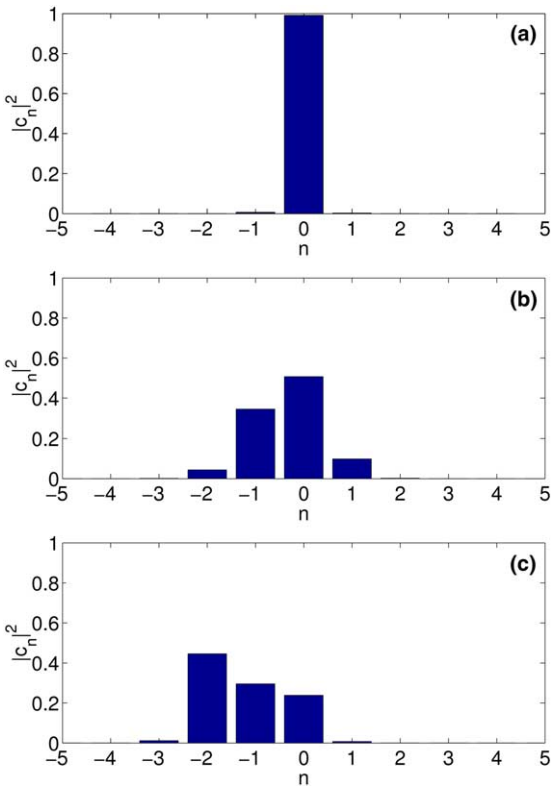

Fig. 4. Momentum distribution $|c_n|^2$ at $z_1 = \overline{L}$ when (a) $\bar{t} = 10$, (b) $\bar{t} = 25$, (c) $\bar{t} = 60$ and $\overline{L} = 0.1$, $\bar{\rho} = 10$ and $\delta = 0$.

parameters as those used in Fig. 3. It shows that in the early stages of the instability both $n = 1$ and $n = -1$ are populated, and that several momentum states are occupied during the course of the instability, with the mean particle momentum becoming progressively more negative.

5.1.2. Quantum limit

We now consider situations in the quantum limit where $\bar{\rho}\overline{L}^{1/2}$ is sufficiently small that the quantum nature of the particle-field interaction becomes significant.

In the case of a short particle sample such that $\overline{L} \ll 1$, the evolution of the field intensity, the bunching parameter b, and the average momentum $\langle p \rangle$ as a function of $\bar{t}$ at the front edge of the particle sample ($z_1 = \overline{L}$) is shown in Fig. 5 for the case where $\overline{L} = 0.1$, $\bar{\rho} = 0.2$ and $\delta = 1$. It can be seen that, similar to the case of a short sample in the classical regime (Fig. 3), the particle sample emits a superradiant pulse, followed by a succession of smaller pulses. There is very close correspondence between the full numerical simulation of Eqs. (24) and (25) shown in Fig. 5 and the solutions of the self-similar equations (44) and (45) shown in Fig. 2(b) and (d). The different time scales of Figs. 3 and 5 for the quantum and the classical regime, respectively, is notable. In fact, in agreement with the definition of the quantum and classical self-similar variables x (43) and y (37), the ratio between the quantum and the classical time scales is $\bar{\rho}\sqrt{\overline{L}}/2 \sim 30$ for $\bar{\rho} = 0.2$ and $\overline{L} = 0.1$. In addition, inspection of Fig. 5(b) and (c) shows that in the quantum case the bunching factor b is zero when $\langle p \rangle = -1$, since in the two-state approximation $b \approx c_0 c_{-1}^*$ is zero when the particles are all in the state $n = -1$.

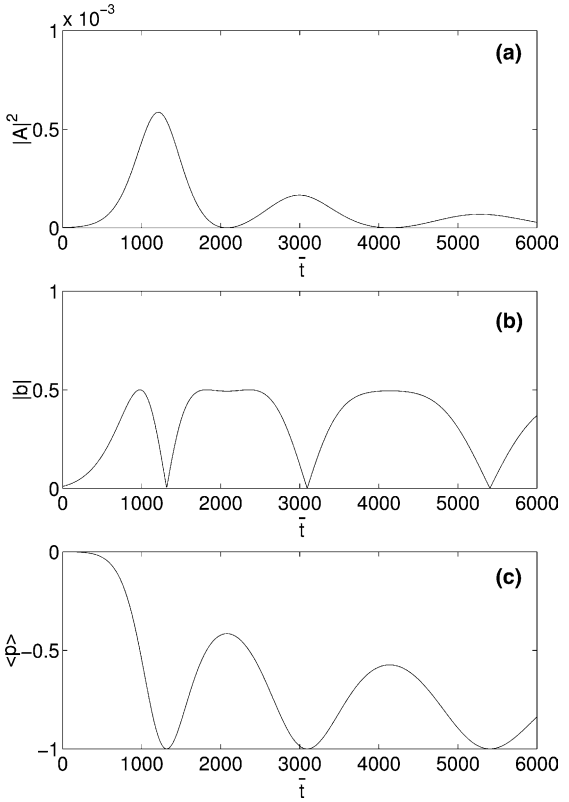

Fig. 5. (a) $|A|^2$, (b) $|b|$ and (c) $\langle p \rangle$ as a function of $\bar{t}$ at $z_1 = \overline{L}$ when $\overline{L} = 0.1$, $\bar{\rho} = 0.2$ and $\delta = 1$.

The main difference between the classical and quantum cases is the distribution of particle momenta (see Figs. 4 and 6): in the quantum regime shown in Fig. 6, the momentum states $n = 0$ and $n = -1$ are the only ones populated throughout the interaction, whereas in the classical regime, many momentum states with both $n > 0$ and $n < 0$ are occupied. Consequently, although the evolution of the scattered radiation is similar in both the quantum and classical regimes, the evolution of the particle dynamics is very different.

5.2. Long samples – strong superradiance

We now investigate the collective recoil instability in long samples such that the particle sample is much greater than the cooperation length i.e. $L \gg L_c$ or $\overline{L} \gg 1$. In such cases, propagation effects are highly significant as radiation emitted at the rear of the sample does not escape rapidly into free space, but undergoes further interaction with parts of the sample towards the front of the particle sample. This regime is most relevant to the FEL, particularly when operating at short wavelengths e.g. X-rays, as typically $\overline{L} \gg 1$.

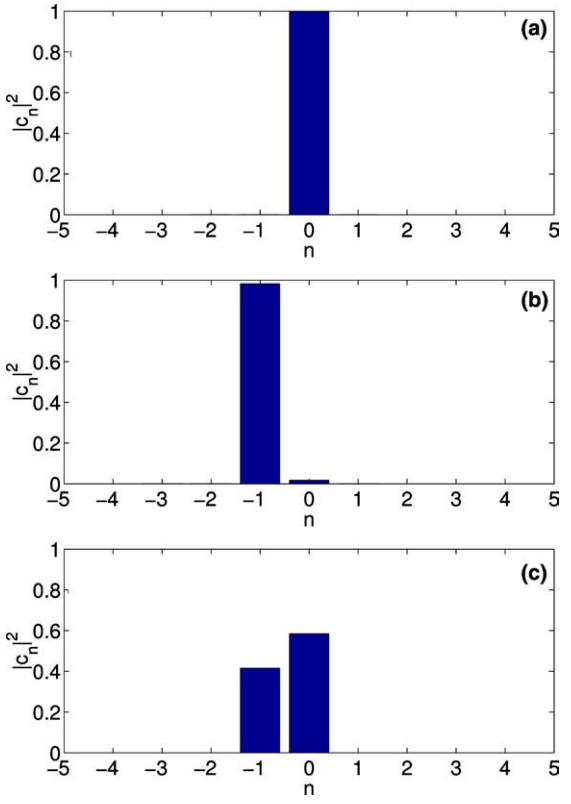

Fig. 6. Momentum distribution $|c_n|^2$ at $z_1 = \overline{L}$ when (a) $\bar{t} = 90$, (b) $\bar{t} = 1260$ and (c) $\bar{t} = 2100$ and $\overline{L} = 0.1$, $\bar{\rho} = 0.2$ and $\delta = 1$. Inspection of Fig. 5 shows that these times correspond to points well before, close to and after the first scattered intensity maximum respectively.

5.2.1. Classical case

Fig. 7 shows the evolution of the scattered field at different times for the case where $\overline{L} = 30$, $\bar{\rho} = 10$ and $\delta = 0$. The particle sample occupies the region $0 < z_1 < \overline{L}$, whereas in the region $z_1 > \overline{L}$ the radiation propagates into free space, escaping from the front edge of the sample $z_1 = \overline{L}$. It can be seen that inside the particle sample there are two distinct regions in which the evolution of the field differs considerably. In the region where $\bar{t} < z_1 < \overline{L}$, the field evolution is spatially uniform and can be described by the mean field model [17,19] or 'steady-state' FEL theory [23]. In this region, the peak scaled intensity $|A|^2$ is independent of $\bar{\rho}$, which implies that the real peak intensity scales as $\propto N^{4/3}$. In contrast, in the region where $0 < z_1 < \bar{t}$, effects of propagation are significant. This region contains a high intensity, narrow pulse or 'spike' of radiation which evolves self-similarly as it travels through the particle sample, increasing in intensity and decreasing in width as it propagates. It can be shown that this pulse is superradiant in character, its peak intensity scaling as $\propto N^2$. A physical explanation for the emergence of this intense superradiant pulse is as follows: At the rear of the pulse $z_1 \to 0$, the particle-field interaction evolves similarly to the case of a short particle sample considered in the previous section. The particles emit a small amplitude superradiant pulse. The emitted field propagates away from these particles towards the front of the sample, but instead of propagating into free space as was the case for a short sample, the pulse propagates forward through the remainder of the sample, being amplified as it propagates. We distinguish this high-intensity superradiant pulse generation from the (much lower intensity) superradiant pulse generation from short samples

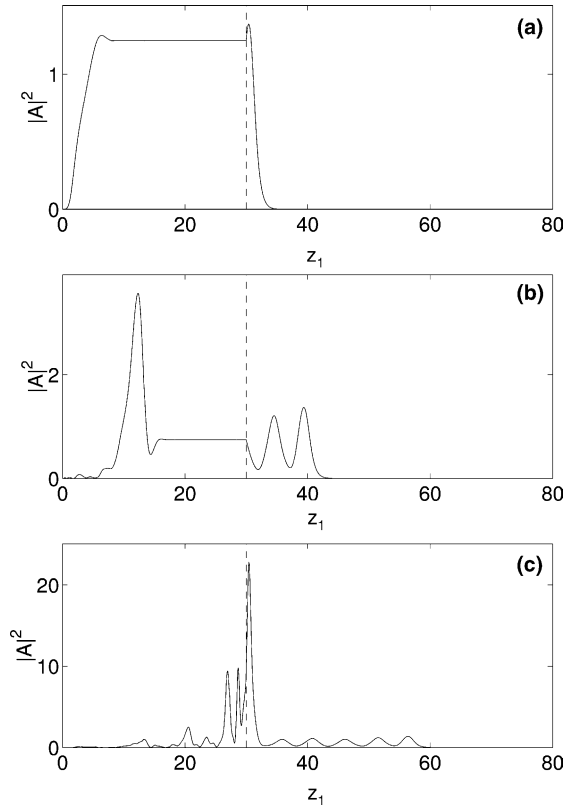

Fig. 7. $|A|^2$ as a function of z_1 at (a) $\bar{t} = 8$, (b) $\bar{t} = 17$ and (c) $\bar{t} = 34$ when $\bar{L} = 30$, $\bar{\rho} = 10$ and $\delta = 0$.

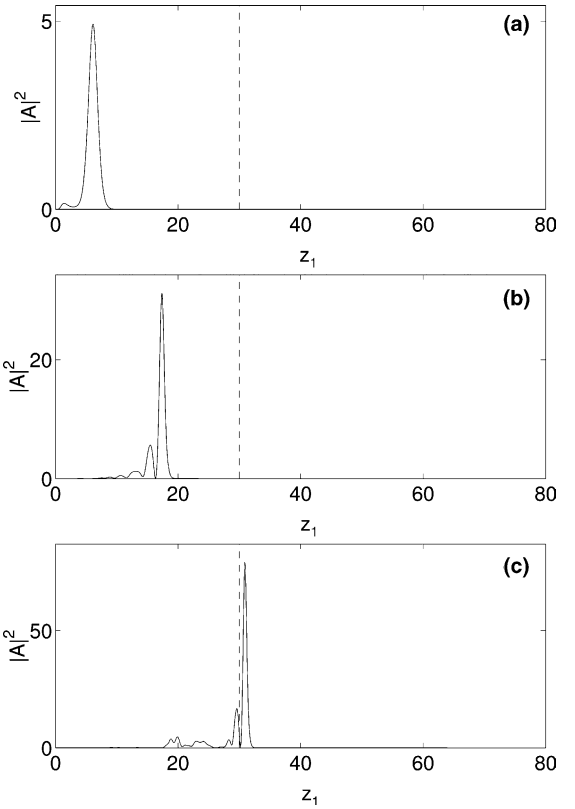

Fig. 8. $|A|^2$ as a function of z_1 at (a) $\bar{t} = 11$, (b) $\bar{t} = 21$ and (c) $\bar{t} = 34$ when $\bar{L} = 30$, $\bar{\rho} = 10$ and $\delta = 2\bar{\rho} = 20$.

by referring to them as 'strong' and 'weak' superradiance respectively.

An interesting feature of the strong superradiant pulses observed here is that they are not sensitive to the pump-probe detuning, δ. This can be explained by the fact that the origin of these pulses is *spontaneous* scattering by the rear part of the sample, which then stimulates further scattering as it propagates and is amplified during its passage forward through the sample. This insensitivity to pump-probe detuning is demonstrated in Fig. 8, which has been obtained using the same parameters as Fig. 7 with the exception that now $\delta = 2\bar{\rho} = 20$. For this value of δ, mean field theory predicts no instability [17,20] as shown by Fig. 1, and it can be seen from Fig. 7 that in the region where $z_1 > \bar{t}$ the field intensity is not amplified. In contrast, in the region in which the effects of propagation are significant, $0 < z_1 < \bar{t}$, the growth of strong superradiant pulses is not significantly affected by the change in δ. In fact, the growth of the superradiant pulse is enhanced as it propagates through 'fresh' particles which have not been perturbed or heated by any significant previous interaction.

Fig. 9 shows the momentum distribution at the front of the sample ($z_1 = \bar{L}$) at different times. The parameters used are the same as those for Fig. 8. It can be seen that the superradiant pulse causes population of a large number of momentum states, with both $n > 0$ and $n < 0$. The effect of the narrow, intense superradiant 'spike' of radiation on the momentum distribution of the particles at the front of the sample as it propagates through them is dramatically illustrated in Fig. 9(b) and (c). Fig. 9(b) shows the momentum distribution at the time

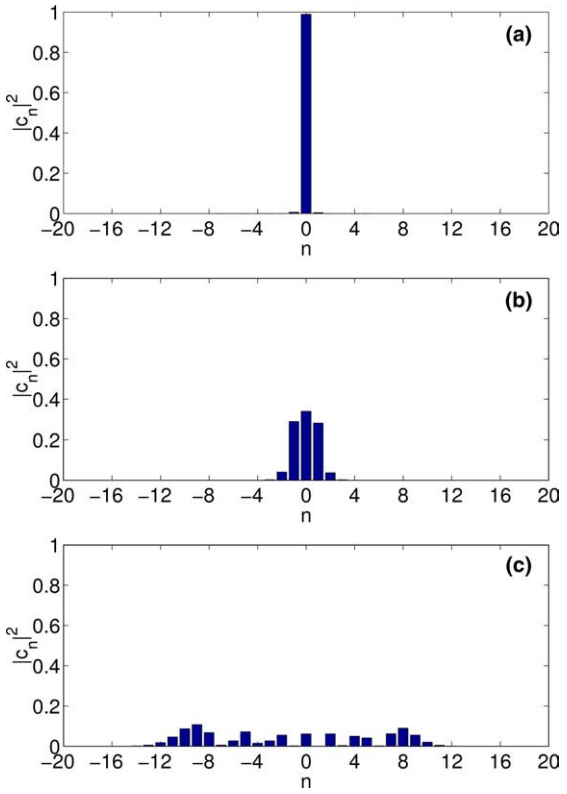

Fig. 9. Momentum distribution $|c_n|^2$ at $z_1 = \overline{L}$ when (a) $\bar{t} = 24$, (b) $\bar{t} = 31.7$ and (c) $\bar{t} = 32.4$ and $\overline{L} = 30$, $\bar{\rho} = 10$ and $\delta = 2\bar{\rho} = 20$.

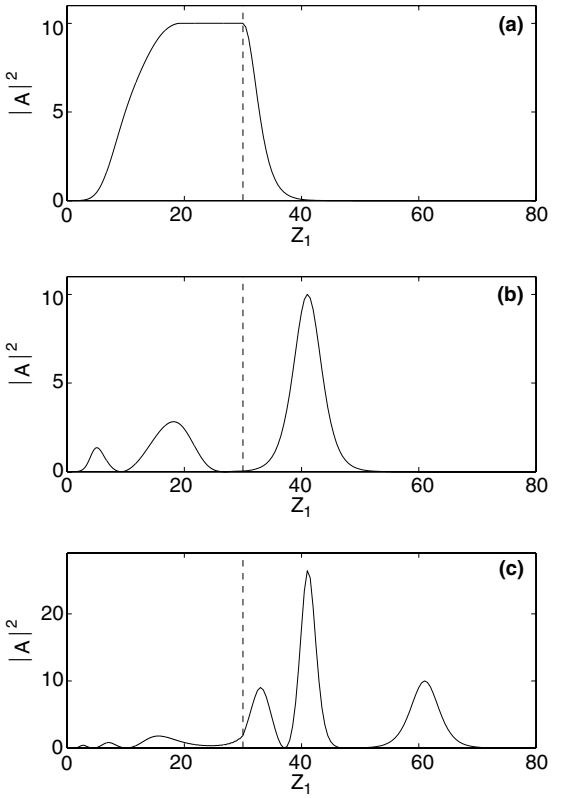

Fig. 10. $|A|^2$ as a function of z_1 at (a) $\bar{t} = 19$, (b) $\bar{t} = 30$ and (c) $\bar{t} = 50$ when $\overline{L} = 30$, $\bar{\rho} = 0.2$ and $\delta = 1$.

immediately after the arrival of the front edge of the spike at $z_1 = \overline{L}$ ($\bar{t} = 31.7$) and Fig. 9(c) shows the momentum distribution after the passage of the spike at $z_1 = \overline{L}$ ($\bar{t} = 32.4$). The width of the momentum distribution at $z_1 = \overline{L}$ can be seen to increase by approximately an order of magnitude during the short transit time of the superradiant spike.

5.2.2. Quantum limit

As for the case of the classical regime, we now consider the effects of propagation in a long sample where $\overline{L} \gg 1$. Fig. 10 shows the scattered field at the front edge of the sample ($z_1 = \overline{L}$) at different times. For regions of the sample such that $\bar{t} < z_1 < \overline{L}$, the scattered field evolves uniformly in space, as predicted by mean field theory [17], which eventually is emitted from the front of the sample as a hyperbolic secant pulse with area 2π (see Fig. 10(b) for $z_1 > 30$). However just as for the case of classical dynamics (see Fig. 7) for $0 < z_1 < \bar{t}$ the radiation emitted spontaneously from the back of the sample propagates through the sample to the front, and the evolution of the field changes in character to a large amplitude superradiant pulse.

As in the classical case (see Fig. 8), the superradiant pulse is not sensitive to the detuning δ. This is demonstrated by Fig. 11, which shows the scattered field evolution for different times for an off-resonant case where the parameters used are the same as for Fig. 10 with the exception that now $\delta = 3\bar{\rho} = 0.6$, for which mean field theory predicts that the system is stable, as shown by Fig. 1. In fact, it can be seen from Fig. 11 that in regions where $\bar{t} < z_1 < \overline{L}$, no spatially uniform amplification of the field occurs. In contrast, the slippage

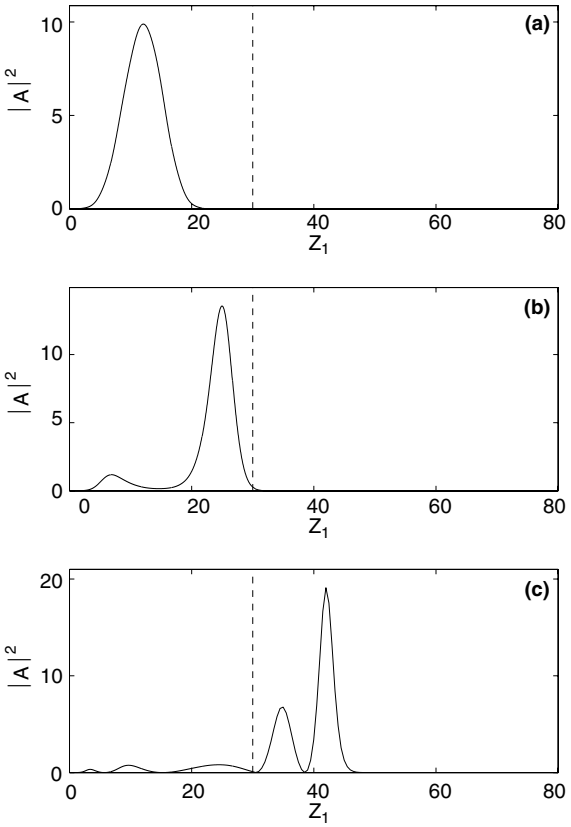

Fig. 11. $|A|^2$ as a function of z_1 at (a) $\bar{t} = 24$, (b) $\bar{t} = 34$ and (c) $\bar{t} = 50$ when $\bar{L} = 30$, $\bar{\rho} = 0.2$ and $\delta = 3\bar{\rho} = 0.6$.

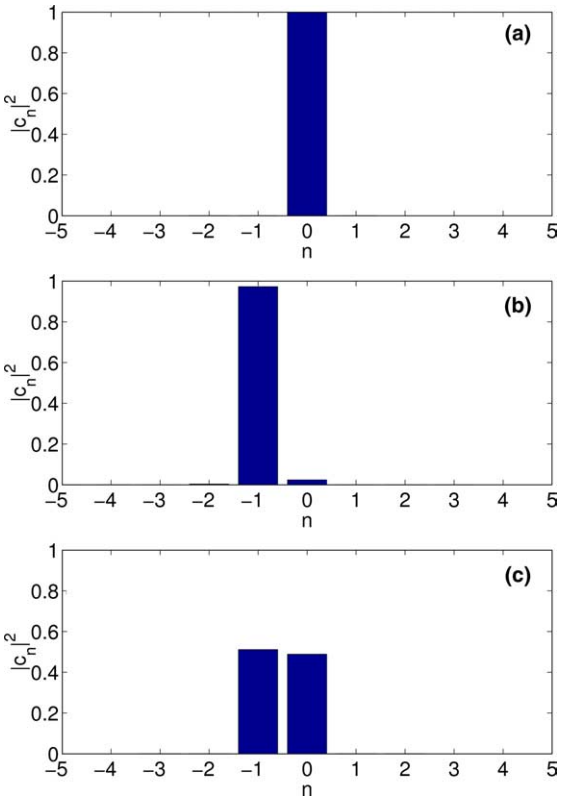

Fig. 12. Momentum distribution $|c_n|^2$ at $z_1 = \bar{L}$ when (a) $\bar{t} = 24$, (b) $\bar{t} = 38.5$ and (c) $\bar{t} = 50$ and $\bar{L} = 30$, $\bar{\rho} = 0.2$ and $\delta = 3\bar{\rho} = 0.6$.

region $0 < z_1 < \bar{t}$ still gives rise to a strong superradiant pulse.

Fig. 12 shows the momentum distribution at the front of the sample ($z_1 = \bar{L}$) at different times which have been chosen to show occasions when the atoms at $z_1 = \bar{L}$ are almost entirely in momentum state $n = 0$ (Fig. 12(a)), almost entirely in momentum state $n = -1$ (Fig. 12(b)) and in a coherent superposition of the momentum states $n = 0$ and $n = -1$ (Fig. 12(c)). The parameters used are the same as those for Fig. 11. It can be seen that in contrast to the case of classical evolution in a long sample (see Fig. 9) only two momentum states, $n = 0$ and $n = -1$, are populated during the interaction. Note that in the case of Fig. 12(c), where there is a coherent superposition of two momentum states, then the atomic system is bunched according to Eq. (26).

6. Conclusions

We have presented a quantum model for collective recoil lasing including the effects of propagation, where the temporal and spatial evolution of the collective recoil lasing process is described. The treatment is based on multiple-scaling perturbation theory, in which the radiation amplitude evolves on a spatial scale much slower than the radiation wavelength. The model depends on a single collective parameter $\bar{\rho}$ which represents the maximum number of photons emitted per particle and rules the transition between the quantum (for $\bar{\rho} \leqslant 1$) and classical (for $\bar{\rho} \gg 1$) regimes. Our results predict that the radiation produced during collective recoil lasing evolves superradiantly with peak intensity proportional to N^2 both in the case where the particle sample is short compared to

the cooperation length of the system, and where the sample is long compared to the cooperation length. In both short and long pulse cases, it is found that there is a classical and quantum regime of superradiant emission. In the case of classical superradiant emission, many momentum states participate in the interaction whereas during quantum superradiant emission only two momentum states participate in the interaction. For short samples in both quantum and classical regimes of evolution, the superradiant pulse is low-intensity 'weak' superradiance. For long pulses in both quantum and classical regimes of evolution the initially weak superradiant pulse emitted in the region near the rear edge of the ensemble evolves with a self-similar profile due to propagation and is strongly amplified as it propagates toward the front edge of the sample. This 'strong' superradiant pulse is shown to have a much higher peak intensity than that predicted by 'mean-field' or 'steady-state' models in which propagation effects are neglected.

The results presented here are relevant both to CARL experiments and FEL experiments. In typical CARL experiments, the sample length is much shorter than the cooperation length ($\overline{L} \ll 1$), the system evolves in the weak superradiant regime, and the superradiant pulses produced have low intensity. It may also be possible to access the long pulse regime and produce high-intensity strong superradiance by using an optical cavity to increase the effective length of the atomic sample. In FEL experiments operating at short wavelengths, typically the electron bunch length is much longer than the cooperation length so that $\overline{L} \gg 1$. Short wavelengths FELs which amplify incoherent shot noise via SASE (self-amplified spontaneous emission) are of great current interest worldwide as potential sources of ultra bright coherent X-ray radiation. Propagation effects and self-similar superradiant spikes are known to be fundamental to SASE [24]. A detailed study of SASE in FELs using a quantum-mechanical description of the electron dynamics will be the subject of a future publication.

The present work neglects transverse propagation effects, which could be relevant in the long-pulse case, as it occurs in the classical regime of FEL [38]. We expect that these effects should be negligible when the Rayleigh range of the radiation pulse is much longer than the gain length. However, a definitive answer to this problem can be provided only by numerically solving the 3D equations, which can be easily obtained generalizing equations (15) and (16). This will be the subject of a future investigation.

Appendix A. Derivation of the multiple-scaling equations (15) and (16)

We now describe the derivation Eqs. (15) and (16). Regarding $A(\theta, z_1, \bar{t})$ and $\Psi(\theta, z_1, \bar{t})$ as depending on $z_1 = \epsilon\theta$ as an extra independent variable and using the chain rule

$$\frac{\partial}{\partial\theta} \to \frac{\partial}{\partial\theta} + \epsilon\frac{\partial}{\partial z_1}, \tag{A.1}$$

Eqs. (1) and (2) become

$$\mathrm{i}\frac{\partial\Psi}{\partial\bar{t}} = -\frac{1}{\bar{\rho}}\left(\frac{\partial^2}{\partial\theta^2} + 2\epsilon\frac{\partial^2}{\partial\theta\partial z_1} + \epsilon^2\frac{\partial^2}{\partial z_1^2}\right)\Psi - \frac{\mathrm{i}\bar{\rho}}{2}\left(A\mathrm{e}^{\mathrm{i}\theta} - \text{c.c.}\right)\Psi, \tag{A.2}$$

$$\epsilon\frac{\partial A}{\partial\bar{t}} + \frac{\partial A}{\partial\theta} + \epsilon\frac{\partial A}{\partial z_1} = \epsilon|\Psi|^2\mathrm{e}^{-\mathrm{i}\theta} + \mathrm{i}\epsilon\bar{\delta}A, \tag{A.3}$$

where $\bar{\delta} = \delta/\bar{\rho}$. Now we insert the perturbation expansion

$$\Psi = \Psi^{(0)} + \epsilon\Psi^{(1)} + \cdots, \tag{A.4}$$

$$A = A^{(0)} + \epsilon A^{(1)} + \cdots \tag{A.5}$$

into Eqs. (A.2) and (A.3) and obtain equations relating the coefficients of the various power of ϵ. In the limit $\epsilon \to 0$ we are only interested in $\Psi^{(0)}$ and $A^{(0)}$.

The zeroth-order of Eq. (A.2) is

$$\mathrm{i}\frac{\partial\Psi^{(0)}(\theta,z_1,\bar{t})}{\partial\bar{t}} = -\frac{1}{\bar{\rho}}\frac{\partial^2}{\partial\theta^2}\Psi^{(0)}(\theta,z_1,\bar{t}) - \frac{\mathrm{i}\bar{\rho}}{2}\left(A^{(0)}(z_1,\bar{t})\mathrm{e}^{\mathrm{i}\theta} - \text{c.c.}\right)\Psi^{(0)}(\theta,z_1,\bar{t}), \tag{A.6}$$

which corresponds to Eq. (15), whereas the zeroth- and first-order of Eq. (A.3) are, respectively,

$$\frac{\partial A^{(0)}}{\partial\theta} = 0, \tag{A.7}$$

$$\frac{\partial A^{(1)}}{\partial\theta} = |\Psi^{(0)}|^2 e^{-i\theta} + i\bar{\delta}A^{(0)} - \left(\frac{\partial A^{(0)}}{\partial \bar{t}} + \frac{\partial A^{(0)}}{\partial z_1}\right). \tag{A.8}$$

Hence, $A^{(0)}(z_1,\bar{t})$ is a slowly varying function of z_1. Integrating both sides of Eq. (A.8) over θ between 0 and 2π and assuming that $A^{(1)}$ is a periodic function of θ, we obtain

$$\frac{\partial A^{(0)}(z_1,\bar{t})}{\partial \bar{t}} + \frac{\partial A^{(0)}(z_1,\bar{t})}{\partial z_1} = \frac{1}{2\pi}\int_0^{2\pi} d\theta\, |\Psi^{(0)}(\theta,z_1,\bar{t})|^2 e^{-i\theta} + i\bar{\delta}A^{(0)}(z_1,\bar{t}), \tag{A.9}$$

which corresponds to Eq. (16).

References

[1] R. Bonifacio, C. Pellegrini, L. Narducci, Opt. Commun. 50 (1984) 373.
[2] R. Bonifacio, L. De Salvo Souza, Nucl. Instrum. Meth. Phys. Res. A 341 (1994) 360.
[3] R. Bonifacio, L. De Salvo Souza, L. Narducci, E.J. D'Angelo, Phys. Rev. A 50 (1994) 1716.
[4] R. Bonifacio, L. De Salvo Souza, Opt. Commun. 115 (1995) 505.
[5] G.L. Lippi, et al., Phys. Rev. Lett. 76 (1996) 2452.
[6] P.R. Hemmer, et al., Phys. Rev. Lett. 77 (1996) 1468.
[7] D. Kruse, C. von Cube, C. Zimmermann, P.W. Courteille, Phys. Rev. Lett. 91 (2003) 183601.
[8] G.R.M. Robb, N. Piovella, A. Ferraro, R. Bonifacio, P.W. Courteille, C. Zimmermann, Phys. Rev. A 69 (2004) 041403(R).
[9] C. von Cube, S. Slama, D. Kruse, C. Zimmermann, Ph.W. Courteille, G.R.M. Robb, N. Piovella, R. Bonifacio, Phys. Rev. Lett. 93 (2004) 083601.
[10] S. Inouye, et al., Science 285 (1999) 571.
[11] M. Kozuma, et al., Science 286 (1999) 2309; S. Inouye, et al., Nature 402 (1999) 641.
[12] R. Bonifacio, F.S. Cataliotti, M. Cola, L. Fallani, C. Fort, N. Piovella, M. Inguscio, Opt. Commun. 233 (2004) 155.
[13] L. Fallani, C. Fort, N. Piovella, M. Cola, F.S. Cataliotti, M. Inguscio, R. Bonifacio, Phys. Rev. A 71 (2005) 033612.
[14] R. Bonifacio, Opt. Commun. 146 (1998) 236.
[15] M.G. Moore, P. Meystre, Phys. Rev. A 58 (1998) 3248.
[16] M.G. Moore, O. Zobay, P. Meystre, Phys. Rev. A 60 (1999) 1491.
[17] N. Piovella, M. Gatelli, R. Bonifacio, Opt. Commun. 194 (2001) 167.
[18] H.Y. Ling, H. Pu, L. Baksmaty, N.P. Bigelow, Phys. Rev. A 63 (2001) 053810.
[19] N. Piovella, M. Gatelli, L. Martinucci, R. Bonifacio, B.W.J. M^{c}Neil, G.R.M. Robb, Laser Phys. 12 (2002) 188.
[20] N. Piovella, M. Cola, R. Bonifacio, Phys. Rev. A 67 (2003) 013817.
[21] R. Bonifacio, G.R.M. Robb, B.W.J. M^{c}Neil, Phys. Rev. A 56 (1997) 912.
[22] R. Bonifacio, B.W.J. McNeil, P. Pierini, Phys. Rev. A 40 (1989) 4467.
[23] R. Bonifacio, F. Casagrande, G. Cerchioni, L. De Salvo Souza, P. Pierini, N. Piovella, Riv. Nuovo Cimento 13 (9) (1990) 1.
[24] R. Bonifacio, L. De Salvo, P. Pierini, N. Piovella, C. Pellegrini, Phys. Rev. Lett. 73 (1994) 70.
[25] J. Andruszkow, et al., Phys. Rev. Lett. 85 (2000) 3825.
[26] S.V. Milton, et al., Science 292 (2001) 2037.
[27] R. Bonifacio, M. Cola, N. Piovella, G.R.M. Robb, Europhys. Lett. 69 (2005) 55.
[28] G. Preparata, Phys. Rev. A 38 (1988) 233.
[29] G.T. Moore, M.O. Scully, Phys. Rev. A 21 (1980) 2000.
[30] J.M.J. Madey, J. Appl. Phys. 42 (1971) 1906.
[31] A. Friedman, A. Gover, G. Kurizki, S. Ruschin, A. Yariv, Rev. Mod. Phys. 60 (1988) 471.
[32] F.T. Arecchi, R. Bonifacio, IEEE Quantum Electron. 1 (1965) 169.
[33] J.A. Murdock, Perturbations: Theory and Methods, John Wiley & Sons, New York, 1991.
[34] D.C. Burnham, R.Y. Chiao, Phys. Rev. 188 (1969) 667.
[35] R. Bonifacio, C. Maroli, N. Piovella, Opt. Commun. 68 (1988) 369.
[36] G.R.M. Robb, N. Piovella, R. Bonifacio, J. Opt. B: Quantum Semiclass. Opt. 7 (2005) 93.
[37] R. Bonifacio, F. Casagrande, Opt. Commun. 50 (1984) 251.
[38] G.T. Moore, Nucl. Instrum. Meth. Phys. Res. A 239 (1985) 19.